analytical chemistry

Article

Cite This: *Anal. Chem.* 2019, 91, 3561−3566

pubs.acs.org/ac

Precise Regulation of Enzyme Cascade Catalytic Efficiency with DNA Tetrahedron as Scaffold for Ultrasensitive Electrochemical Detection of DNA

Ding Wang, Yaqin Chai, Yali Yuan,* and Ruo Yuan*

Supporting Information

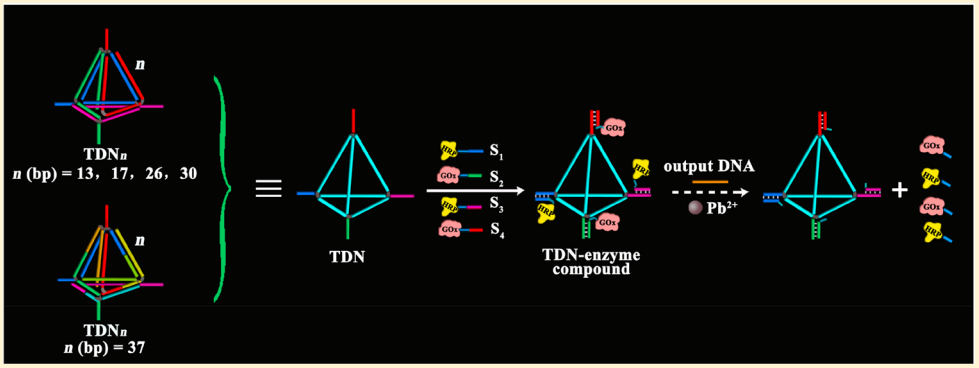

ABSTRACT: In this work, a rigid DNA tetrahedron (TDN) scaffold was synthesized to precisely control the interenzyme distance by randomly anchoring two pairs of horseradish peroxidase (HRP)/glucose oxidase (GOx) at the vertices of TDN, which could not only avoid the drawbacks of poor controllability and biocompatibility from traditional scleroid skeletons, but also overcome the defect of imprecise regulation for interenzyme distance caused by DNA origami. Impressively, by varying the side length of TDN scaffold, the interenzyme distance was precisely regulated, thus, an optimal TDN scaffold with highest catalytic efficiency was acquired and subsequently applied for constructing an ultrasensitive biosensor for DNA detection with a low detection limit of 3 fM. This strategy paved an avenue for developing new reliable scaffold to precisely regulate the catalytic efficiency of enzyme cascade reaction with ultimate applications in bioanalysis and clinical diagnosis.

In living system, myriads of delicate enzyme cascade reactions involving molecules production and energy harvest, play a vital role in the metabolism and propagation processes, in which the reaction efficiency relies on the appropriate distance regulation of participating enzymes on a scaffold (e.g., cytoskeleton or cell membrane).[1−8] However, it is difficult to achieve precise regulation for the interenzyme distance in vitro owing to the lack of reliable scaffolds for locating multienzymes.[9−12] Recently, some scleroid skeletons are applied for regulating the interenzyme distance to improve the efficiency of enzyme cascade reactions.[13−17] Nevertheless, they inevitably involve some drawbacks of poor controllability and biocompatibility, thus, it is hard to precisely regulate the interenzyme distance, resulting in obstacle to obtain high efficient enzyme cascade reaction.[18−20] Very recently, Yan's group ruled the distance between two addressable fulcrums on DNA origami for achieving efficient enzyme cascade reaction, in which different enzymes were immobilized on fulcrums via the hybridization of single DNA labeled on different enzymes with the single DNA attached on fulcrums.[21,22] Although the distance of two addressable fulcrums can be precisely regulated here, it is difficult to precisely control the interenzyme distance owing to the swing tendency of flexible DNA,[23−27] resulting in the restriction to determine optimal interenzyme distance for highly efficient enzyme cascade reaction. Therefore, it is significantly desirable to pursuit a reliable scaffold with good biocompatibility and controllability for precisely regulating interenzyme distance and obtaining the optimal enzyme cascade catalytic efficiency.

To address these issues, in this paper, a DNA tetrahedron (TDN) scaffold with good biocompatibility and controllability was used to anchor model enzymes (HRP/GOx) to the vertices of TDN, realizing precise regulation of interenzyme distance for highly efficient enzyme cascade reaction. Compared with traditional scaffolds, the TDN scaffold could not only avoid the drawbacks of poor controllability and biocompatibility from scleroid skeletons, but also overcome the defect of imprecise regulation for interenzyme distance from DNA origami. Additionally, by varying the side length of TDN scaffold, the interenzyme distance was precisely regulated, and an enzyme cascade reaction with highest catalytic efficiency was acquired. As a proof of concept, an electrochemical assay exhibiting obvious advantages in high sensitivity, low cost, fast response, and simple instrumentation was developed for DNA detection.

Received: November 22, 2018
Accepted: February 13, 2019
Published: February 13, 2019

DOI: 10.1021/acs.analchem.8b05407
Anal. Chem. 2019, 91, 3561−3566

Scheme 1. (A) Preparation of DNA Tetrahedron (TDN) Scaffolds for Regulation of Interenzyme Distance between HRP and GOx; (B) Exo III-Assisted Target Cycling Amplification Section; (C) Switching of the Enzyme Cascade Catalytic Signal for Target Analysis

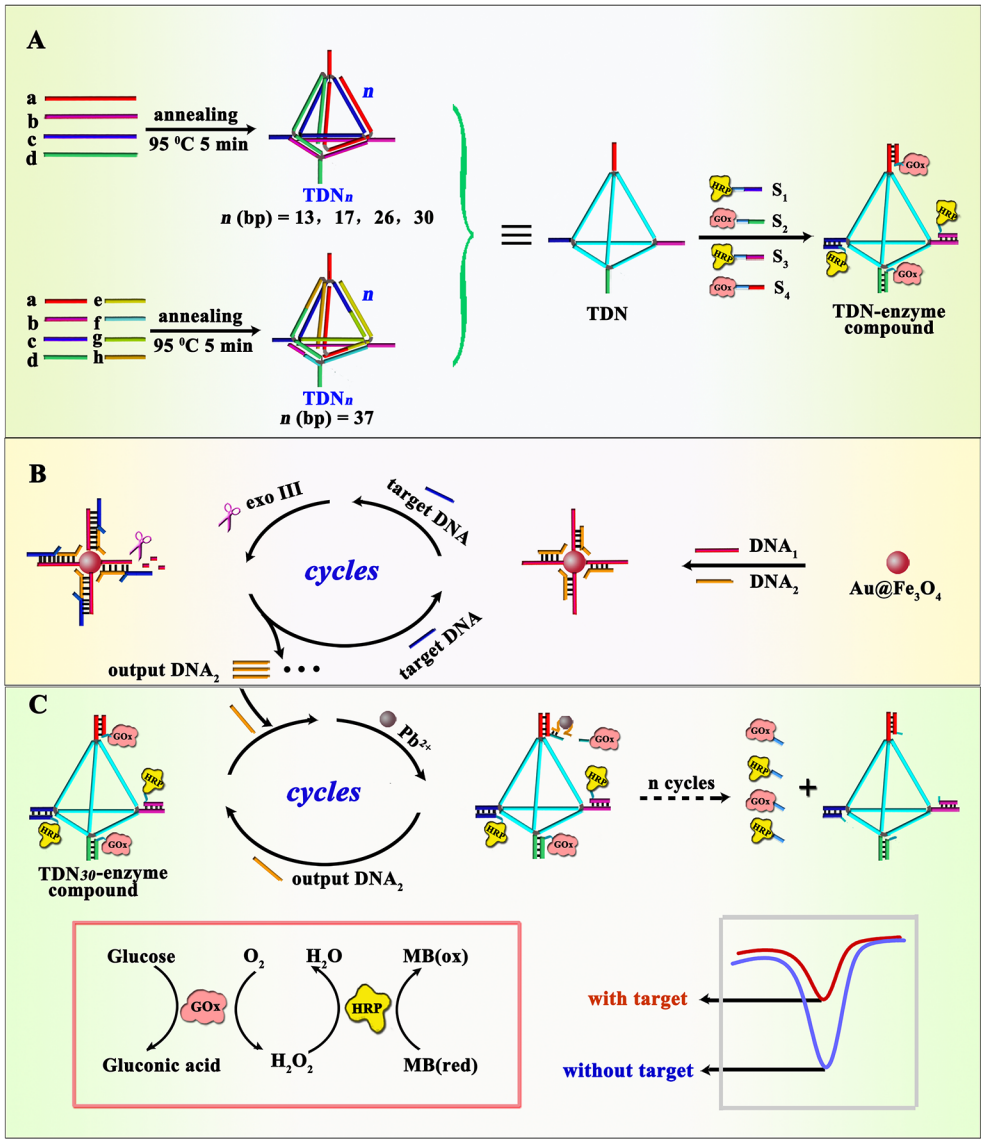

In this context, five TDN scaffolds (TDN_{13}, TDN_{17}, TDN_{26}, TDN_{30}, and TDN_{37}) with different sizes had been designed for systematically regulating the interenzyme distance between GOx and HRP, in which each edge of the TDN contained 13, 17, 26, 30, or 37 base pairs, respectively (Scheme 1A). The optimal TDN scaffold (TDN_{30}) with highest catalytic efficiency was evaluated, and it was further applied in the construction of an electrochemical biosensor for target DNA (a fragment sequence of p53 gene) detection. Here, exonuclease III (Exo III)-assisted cycling amplification strategy was employed (Scheme 1B), which converted small amounts of target DNA into massive output DNA_2 (a Pb^{2+}-dependent DNAzyme). Subsequently, the output DNAzyme hybridized with its substrate that the identical DNA fragments possessed by enzyme-modified DNA (S_1, S_2, S_3, S_4). With the help of cofactor Pb^{2+}, DNAzyme cleaved the substrate, thereby releasing the enzyme-modified segment from substrate. Switching of the enzyme cascade catalytic signal accompanied the change of interenzyme distance, enabling the ultrasensitive detection for target DNA (Scheme 1C). Meanwhile, this protocol provided new insights into the development of reliable scaffold to precisely regulate enzyme cascade reaction for early cancer diagnosis and sensing analysis.

EXPERIMENTAL SECTION

Materials and Reagents. Horseradish peroxidase (HRP), *N*-succinimidyl-3-(2-pyridyldithiol) propionate (SPDP), D,L-dithiothreitol (DTT), and glucose oxidase (GOx) were purchased from Sigma (St. Louis, MO, U.S.A.). Methylene blue (MB) and glucose were ordered from Shanghai Aladdin Industrial Corporation (Shanghai, China). Exonuclease III (EXO III) and its buffer were from New England Biolabs (Beijing, China). Magnetic nanoparticles (Fe_3O_4NPs, 100 mg·mL^{-1}) was obtained from Tianjin Baseline Chromtech Research Centre (Tianjin, China). All DNA oligonucleotides were from Sangon Biological Engineering Technology (Shanghai, China) using a high-performance liquid chromato-

DOI: 10.1021/acs.analchem.8b05407
Anal. Chem. 2019, 91, 3561−3566

graph, and their base sequences were shown in Table S1 (see the Supporting Information).

Test and Measurement Equipment. Gels image was carried out on Bio-Rad imaging system (Hercules, CA, U.S.A.). Transmission electron microscopy (TEM) was performed on a JEM-2100F electron microscope (JEOL, Japan). Atomic force microscope (AFM) was carried on a multimode 8 microscope (Bruker, Germany). CHI 660E electrochemistry workstation (Shanghai Chenhua instrument, China) with traditional three-electrode system[28] was used to operate differential pulse voltammetry (DPV) measurements. DPV measurements were performed in 0.1 M PBS solution (pH 7.0) with the potential from −0.5 to 0.1 V, the step potential of 4 mV and the amplitude of 50 mV.

Preparation of Enzyme-Modified DNA. According to some classic enzyme modification methods,[29,30] here, SPDP was chosen to cross-link GOx and HRP with different thiol-modified single strand DNA, including S_1, S_2, S_3, and S_4. First, enzyme solution was activated with SPDP at room temperature for 2 h, which allowed amine-reactive N-hydroxysuccinimide (NHS) esters to react with the lysine residues on enzyme surface. The excess SPDP then was removed by using a Microcon centrifugal filter unit (30 kDa cutoff). In parallel, 10-fold excess thiol-modified single-stranded DNA was incubated with DTT at room temperature for 2 h to cut the S−S bond. Next, SPDP-activated enzyme was conjugated to treated DNA through a disulfide bond exchange of the activated pyridyldithiol group. Based on these procedures, four enzyme-modified DNA conjugations, including GOx-S_1, HRP-S_2, GOx-S_3, and HRP-S_4, were prepared and stored at 4 °C for subsequent usage.

Construction of the TDN-Enzyme Compound. First, five types of TDN scaffolds (TDN_{13}, TDN_{17}, TDN_{26}, TDN_{30}, and TDN_{37}) with different sizes were prepared, in which each edge of the TDN contains 13, 17, 26, 30, or 37 base pairs, respectively. For the assembly of TDN_{13}, TDN_{17}, TDN_{26}, and TDN_{30}, four single-stranded DNA (a, b, c, and d) with an equal molar ratio were mixed in TM buffer (20 mM Tris-HCl, 50 mM $MgCl_2$, pH 8.0) at 95 °C and then cooled to 4 °C. Specially, here, to prevent the formation of undesired secondary structures for the long edges, TDN_{37} was prepared by mixing eight single-stranded DNA (a, b, c, d, e, f, g, and h). After that, prepared TDN was mixed with enzyme-modified DNA, and the mixture reacted for 2 h at room temperature. Here, each TDN carries four pendant DNA at four vertices, which could randomly hybridize with aforementioned GOx-S_1, HRP-S_2, GOx-S_3, and HRP-S_4 for anchoring two pairs of HRP/GOx to the vertices of TDN scaffold, finally obtaining the TDN-enzyme compound.

Exo III-Assisted Target Cycling Amplification Reaction. First, 20 μL of amine-modified DNA_1 incubated with 20 μL of Au@Fe_3O_4[31] solution for 12 h under stirring to covalently couple DNA_1 on the Au@Fe_3O_4 surface via Au−N bond. After rinsing twice with PBS buffer, this conjunction was resuspended in PBS solution. Subsequently, DNA_2 was introduced into above solution and reacted 2 h at room temperature, which hybridized with the DNA_1 to form duplex DNA with a bare 3′terminus at the DNA_2. After another magnetic separation and dispersion, 1 unit·μL^{-1} Exo III, and target DNA with variable concentrations were further added into above solution, followed by incubating at 37 °C for 1 h. The mixture then was heated to 80 °C for 20 min to inactivate Exo III. Finally, the obtained solution was stored at 4 °C before it was used.

DNAzyme-Induced Cycling Cleavage Process. With Exo III-assisted target cycling strategy, small amounts of target DNA could be converted into numerous output DNA_2 (a Pb^{2+}-dependent DNAzyme). The output DNAzyme then mixed with TDN-enzyme compound and reacted at room temperature for 2 h. In this process, output DNAzyme successfully hybridized with its substrate that the identical DNA fragments possessed by enzyme-modified DNA (S_1, S_2, S_3, S_4). With the assistance of cofactor Pb^{2+}, output DNAzyme catalyzed the cleavage of ribonucleobase (rA) in the substrates (S_1, S_2, S_3, S_4), leading to the release of enzyme-modified segments from TDN-enzyme compound.

Polyacrylamide-Gel Electrophoresis (PAGE). The 8% fresh polyacrylamide gel was prepared using 5 × TBE buffer. After DNA samples mixing with the DNA-loading buffer (volume ratio 5:1), the electrophoresis ran about 1.5 h in 1× TBE buffer.

RESULTS AND DISCUSSION

Native PAGE Characterization of TDNs with Different Sizes. In order to demonstrate the assemble process of TDNs with different sizes, native polyacrylamide gel electrophoresis (PAGE, 8%) was applied for identifying their electrophoretic mobility. The results were shown in Figure 1. Figure 1A−E were the PAGE analysis for different TDNs, including TDN_{13},

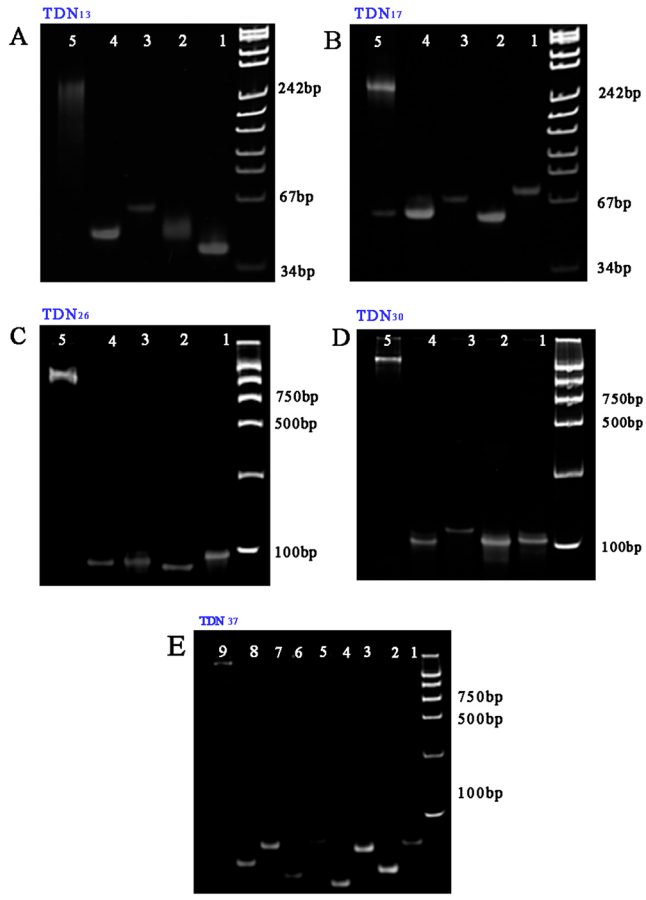

Figure 1. PAGE analysis for the preparation of different TDNs, including TDN_{13} (A), TDN_{17} (B), TDN_{26} (C), TDN_{30} (D), and TDN_{37} (E), respectively.

DOI: 10.1021/acs.analchem.8b05407
Anal. Chem. 2019, 91, 3561−3566

TDN_{17}, TDN_{26}, TDN_{30}, and TDN_{37}, respectively. For the assembly of TDN_{13}, TDN_{17}, TDN_{26}, and TDN_{30}, lanes 1, 2, 3, and 4 represented the distinct single-strand DNA (a−d), respectively. After four single-strand DNA were mixed, bright bands appeared and they migrated more slowly than single strand DNA, suggesting the successful formation of TDN. Especially, for TDN_{37}, eight single strand DNA were designed for DNA assembly. Here, lanes 1−8 showed the single DNA (a−h), respectively, and the bright band at the top of lane 9 was the assemble product of TDN_{37}. Additionally, we observed a decrease of migration rate for assembly products with the increasing size of the TDNs, which further indicated that the successful preparation of differently sized TDNs.

Effect of Different TDN Scaffolds on Enzyme Cascade Catalytic Efficiency. The catalytic efficiency of enzyme cascade reaction was highly depended on the distance of two enzymes (GOx/HRP). To prove this point, TDN scaffolds with different sizes were prepared for precisely regulating enzyme cascade catalytic efficiency and the corresponding DPV responses were depicted in Figure 2. Herein, the TDN_{30}

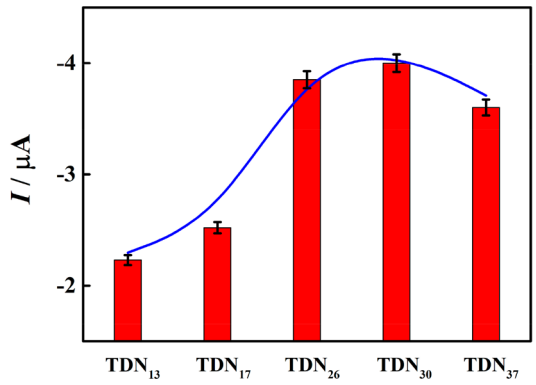

Figure 2. Effect of TDNs with different sizes on electrochemical response. Detection buffer: PBS solution (PH 7.0) containing 4 μM MB (30 μL), 2.0 mM glucose (40 μL), and different TDN-enzyme scaffolds (50 μL).

scaffold (~10.2 nm) exhibited the highest catalytic efficiency against that of TDN_{13} (~4.4 nm), TDN_{17} (~5.8 nm), TDN_{26} (~8.8 nm), and TDN_{37} (~12.6 nm), which may be attributed to that TDN_{30} could avoid diffusion effect and crowding effect to some extent. Therefore, TDN_{30} was chosen as the optimal distance regulation scaffold for efficiently catalyzing enzyme cascade reaction. Furthermore, atomic force microscopy (AFM) was employed to observe the thickness of the assembled optimal TDN scaffold (TDN_{30}). As shown in Figure S1 (see the Supporting Information), a white line profile painted on the AFM image (Figure S1A) exhibited that the thickness is about 10 nm (Figure S1B), which is consistent with the side length of TDN_{30} (~10.2 nm), indicating the successful assembly of TDN_{30} scaffold.

Verification of Enzyme Cascade Reaction. To demonstrate the enzyme cascade catalytic reaction, control experiments were conducted and the results were listed in Figure 3. When the GCE was immersed into the detection buffer of PBS solution containing MB, glucose, and TDN_{30}, a low electrochemical response (Figure 3A) was measured. After unassembled enzyme-modified DNA, including GOx-S_1, HRP-S_2, GOx-S_3, and HRP-S_4, were added into above detection buffer, an enhanced electrochemical response was

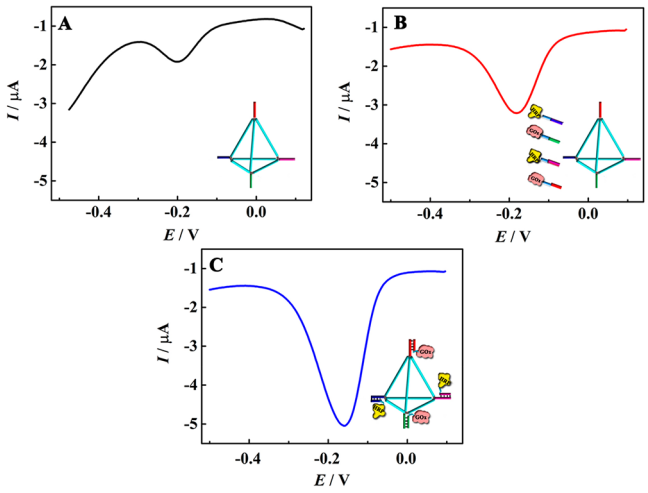

Figure 3. DPV responses of biosensor in different detection buffer: PBS buffer containing 4 μM MB, 2 mM glucose, and TDN_{30} (A); PBS buffer containing 4 μM MB, 2 mM glucose, TDN_{30}, and unassembled enzyme-modified DNA (B); PBS buffer containing 4 μM MB, 2 mM glucose, and TDN_{30} regulated multienzyme compound (C).

observed (Figure 3B), suggesting the enzyme cascade catalytic reaction occurred. What's more, after enzyme-modified DNA were simultaneously assembled on the optimal TDN scaffold (TDN_{30}) and then introduced into detection buffer containing MB and glucose, a highest electrochemical signal (Figure 3C) was obtained, which could be attributed to the reason that the optimal regulation of interenzyme distance could significantly improve enzyme cascade catalytic efficiency.

In order to further explore the enzyme cascade amplification, different electrochemical responses of biosensor in the absence and presence of 2 mM glucose also were researched. Clearly seen in Figure 4, in the absence of glucose, a weak

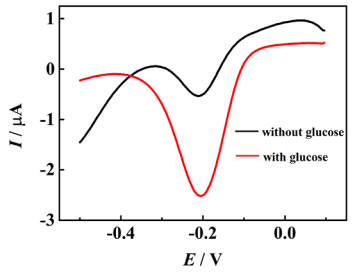

Figure 4. DPV responses of biosensor in the absence and presence of glucose (2 mM) in the PBS solution containing MB (4 μM) and TDN_{30}-enzyme compound.

electrochemical response appeared. However, the electrochemical response increased obviously after the addition of glucose. This was because GOx had catalyzed glucose in detection buffer to generate gluconic acid and hydrogen peroxide. And the hydrogen peroxide, as substrate of HRP, could be further catalytically reduced into H_2O, which in the meantime turned for accelerating the oxidation of electron media MB in detection buffer, finally obtaining the amplified electrochemical response.

Performance Analysis for Proposed Biosensor. In order to assess the sensitivity of proposed method, under optimal conditions (Figure S3, see the Supporting Information), DPV responses of proposed biosensor toward different

DOI: 10.1021/acs.analchem.8b05407
Anal. Chem. 2019, 91, 3561−3566

concentrations of target DNA (a fragment sequence of p53 gene) were investigated. The results were shown in Figure 5.

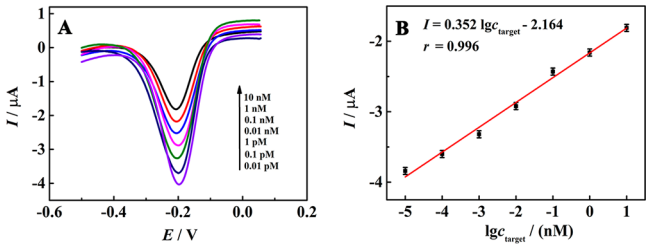

Figure 5. (A) DPV responses of biosensor with different target concentrations (0.01 pM, 0.1 pM, 1 pM, 0.01 nM, 0.1 nM, 1 nM, 10 nM). (B) Calibration plot of currents vs the logarithm (lg) of target DNA concentrations.

The current response was proportional to the logarithm (log) of target DNA concentration from 0.01 pM to 10 nM with a regression equation expressed as $I = 0.352 \lg c_{target} - 2.164$, and the detection limit was calculated to be 3 fM (LOD = $3S_b/m$, where m is the slope of the corresponding calibration curve and S_b is the standard deviation of the blank signals). Additionally, the proposed biosensor also exhibited a remarkable analysis performance in comparison with previously reported methods (Table 1). So we could conclude that the precise regulation of interenzyme distance greatly improved enzyme cascade reaction and enhanced the sensitivity of proposed biosensor.

Table 1. Comparison of Proposed Biosensor with Other Reported Works for DNA Detection

analytical method	detection limit	linear range	ref
colorimetric	5 pM	10−500 pM	32
fluorescent	3.5 pM	10−200 pM	33
fluorescent	5 nM	5−100 nM	34
electrochemical	1 pM	1−800 pM	35
electrochemical	0.12 pM	0.5−80 pM	36
electrochemical	100 fM	0.0001−10 nM	37
electrochemical	3 fM	0.01 pM−10 nM	this work

Preliminary Application of Proposed Biosensor. Standard addition method was applied to evaluate the applicability of proposed biosensor. Here, different concentrations of target DNA (0.01, 0.1, 1.0, and 10 nM) spiked in 50-fold diluted healthy serum were measured. As listed in Table S2 (see the Supporting Information), recovery ranged from 94.1% to 100.5% and the RSD varied from 2.3% to 5.3%, indicating that proposed biosensor was promising for detection target in real samples.

Additionally, as important properties for the electrochemical assay, the stability, reproducibility and specificity of biosensor were evaluated in this work. Herein, the stability of proposed biosensor was challenged via storing it for 15 days. This biosensor still retained 92.5% of its initial electrochemical response, which demonstrated its satisfactory stability. The reproducibility experiments had been studied by interassay (four electrodes were performed with 1 pM target) and intra-assay (the same electrode toward 1 pM target was detected for four times). The RSD were 5.2% and 4.7%, respectively, suggesting good reproducibility of the biosensor. In order to valuate the specificity of the proposed sensing system, various mutants of target DNA, including single-base mismatch sequence (M1), two-base mismatch sequence (M2), and three-base mismatch sequence (M3), were employed as interfering substances. As shown in Figure 6, target DNA

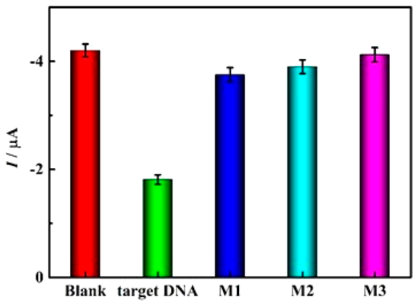

Figure 6. Electrochemical responses of proposed biosensor incubated with different sequences: target DNA (0.01 pM), single-base mismatch sequence (M1, 1 pM), two-base mismatch sequence (M2, 1 pM), and three-base mismatch sequence (M3, 1 pM).

caused significant signal change in comparison with that of blank, while the M1, M2, and M3 at 100-fold concentration caused negligible signal change. These results demonstrated the excellent selectivity of the proposed method for target detection.

CONCLUSION

In summary, a simple, efficient TDN scaffold was used to precisely regulate the interenzyme distance for highly efficient enzyme cascade reaction. Compared with previously reported scaffolds, the new developed TDN scaffold could offer the following combined advantages. First, the TDN scaffold could be easily synthesized based on Watson−Crick base pairing, which exhibited better controllability and biocompatibility than scleroid skeletons. Second, since model enzymes were anchored to the vertices of the TDN scaffold by hybridization of enzyme-modified DNAs with the pendants of TDN, this strategy performed more precise regulation for interenzyme distance than DNA origami. What's more, the described TDN scaffold provided a versatile platform to construct novel biosensor for ultimate application in early cancer diagnosis and sensing analysis.

ASSOCIATED CONTENT

Supporting Information

The Supporting Information is available free of charge on the ACS Publications website at DOI: 10.1021/acs.analchem.8b05407.

Experimental details for the oligonucleotides sequences used in this work (Table S1), AFM characterizations of the TDN_{30} scaffold (Figure S1), the stability verification for TDN-enzyme compound (Figure S2), exploration of experimental conditions (Figure S3), and determination of target added in human serums ($n = 3$) with developed biosensor (Table S2) (PDF).

AUTHOR INFORMATION

Corresponding Authors

*Tel.: +86-23-68252277. Fax: +86-23-68253172. E-mail: y198688@swu.edu.cn.

*E-mail: yuanruo@swu.edu.cn.

DOI: 10.1021/acs.analchem.8b05407
Anal. Chem. 2019, 91, 3561−3566

ORCID

Yaqin Chai: 0000-0003-4392-9592

Ruo Yuan: 0000-0003-3664-6236

Notes

The authors declare no competing financial interest.

■ ACKNOWLEDGMENTS

This work was financially supported by the NNSF of China (21505107, 21775124, and 21575116), the Natural Science Foundation Project of CQ_CSTC (cstc2016jcyjA0189), and the Fundamental Research Funds for the Central Universities (SWU115037, XDJK2018AA003).

■ REFERENCES

(1) Krall, A. S.; Christofk, H. R. *Nature* **2017**, *546*, 357−358.
(2) Kim, T. H.; Mehrabi, P.; Ren, Z.; Sljoka, A.; Ing, C.; Bezginov, A.; Ye, L. B.; Pomes, R.; Prosser, R. S.; Pai, E. F. *Science* **2017**, *355*, 263−275.
(3) Fu, J. L.; Yang, Y. R.; Dhakal, S.; Zhao, Z.; Liu, M. H.; Zhang, T.; Walter, N. G.; Yan, H. *Nat. Protoc.* **2016**, *11*, 2243−2273.
(4) Zhao, Z.; Fu, J. L.; Dhakal, S.; Johnson-Buck, A.; Liu, M. H.; Zhang, T.; Woodbury, N. W.; Liu, Y.; Walter, N. G.; Yan, H. *Nat. Commun.* **2016**, *7*, 10619.
(5) Kuchler, A.; Yoshimoto, M.; Luginbuhl, S.; Mavelli, F.; Walde, P. *Nat. Nanotechnol.* **2016**, *11*, 409−420.
(6) Kim, S. H.; Kim, K. R.; Ahn, D. R.; Lee, J. E.; Yang, E. G.; Kim, S. Y. *ACS Nano* **2017**, *11*, 9352−9359.
(7) Ngo, T. A.; Nakata, E.; Saimura, M.; Morii, T. *J. Am. Chem. Soc.* **2016**, *138*, 3012−3021.
(8) Kou, B. B.; Chai, Y. Q.; Yuan, Y. L.; Yuan, R. *Anal. Chem.* **2017**, *89*, 9383−9387.
(9) Oh, S. W.; Pereira, A.; Zhang, T.; Li, T. R.; Lane, A.; Fu, J. L. *Angew. Chem., Int. Ed.* **2018**, *57*, 1−6.
(10) Peri-Naor, R.; Ilani, T.; Motiei, L.; Margulies, D. *J. Am. Chem. Soc.* **2015**, *137*, 9507−9510.
(11) Peschke, T.; Rabe, K. S.; Niemeyer, C. M. *Angew. Chem., Int. Ed.* **2017**, *56*, 2183−2186.
(12) Zhang, G. Q.; Quin, M. B.; Schmidt-Dannert, C. *ACS Catal.* **2018**, *8*, 5611−5620.
(13) Lian, X. Z.; Chen, Y. P.; Liu, T. F.; Zhou, H. C. *Chem. Sci.* **2016**, *7*, 6969−6973.
(14) Xia, L.; Nguyen, K. V.; Holade, Y.; Han, H.; Dooley, K.; Atanassov, P.; Banta, S.; Minteer, S. D. *ACS Energy Lett.* **2017**, *2*, 1435−1438.
(15) Wang, X. L.; Li, Z.; Shi, J.; Wu, H.; Jiang, Z.; Zhang, W.; Song, X.; Ai, Q. *ACS Catal.* **2014**, *4*, 962−972.
(16) Garcia-Galan, C.; Berenguer-Murcia, A.; Fernandez-Lafuente, R.; Rodrigues, R. C. *Adv. Synth. Catal.* **2011**, *353*, 2885−2904.
(17) Jia, F.; Narasimhan, B.; Mallapragada, S. *Biotechnol. Bioeng.* **2014**, *111*, 209−222.
(18) Fiedler, J. D.; Brown, S. D.; Lau, J. L.; Finn, M. G. *Angew. Chem., Int. Ed.* **2010**, *49*, 9648−9651.
(19) Comellas-Aragones, M.; Engelkamp, H.; Claessen, V. I.; Sommerdijk, N. A. J. M.; Rowan, A. E.; Christianen, P. C. M.; Maan, J. C.; Verduin, B. J. M.; Cornelissen, J. J. L. M.; Nolte, R. J. M. *Nat. Nanotechnol.* **2007**, *2*, 635−639.
(20) Vriezema, D. M.; Aragones, M. C.; Elemans, J. A. A. W.; Cornelissen, J. J. L. M.; Rowan, A. E.; Nolte, R. J. M. *Chem. Rev.* **2005**, *105*, 1445−1489.
(21) Chen, Y. H.; Ke, G. L.; Ma, Y. L.; Zhu, Z.; Liu, M. H.; Liu, Y.; Yan, H.; Yang, C. J. *J. Am. Chem. Soc.* **2018**, *140*, 8990−8996.
(22) Fu, J. L.; Liu, M. H.; Liu, Y.; Woodbury, N. W.; Yan, H. *J. Am. Chem. Soc.* **2012**, *134*, 5516−5519.
(23) Zhang, T.; Hartl, C.; Frank, K.; Heuer-Jungemann, A.; Fischer, S.; Nickels, P. C.; Nickel, B.; Liedl, T. *Adv. Mater.* **2018**, *30*, 1800273.
(24) Tokura, Y.; Harvey, S.; Chen, C. J.; Wu, Y. Z.; Ng, D. Y. W.; Weil, T. *Angew. Chem., Int. Ed.* **2018**, *57*, 1587−1591.
(25) Urban, M. J.; Both, S.; Zhou, C.; Kuzyk, A.; Lindfors, K.; Weiss, T.; Liu, N. *Nat. Commun.* **2018**, *9*, 1454.
(26) Cinti, S.; Proietti, E.; Casotto, F.; Moscone, D.; Arduini, F. *Anal. Chem.* **2018**, *90*, 13680−13686.
(27) Xiong, E. H.; Li, Z. Z.; Zhang, X. H.; Zhou, J. W.; Yan, X. X.; Liu, W. Q.; Chen, J. H. *Anal. Chem.* **2017**, *89*, 8830−8835.
(28) Zhang, P.; Jiang, J.; Yuan, R.; Zhuo, Y.; Chai, Y. Q. *J. Am. Chem. Soc.* **2018**, *140*, 9361−9364.
(29) Hu, Y. W.; Wang, F.; Lu, C. H.; Girsh, J.; Golub, E.; Willner, I. *Chem. - Eur. J.* **2014**, *20*, 16203−16209.
(30) Ke, G. L.; Liu, M. H.; Jiang, S. X.; Qi, X. D.; Yang, Y. R.; Wootten, S.; Zhang, F.; Zhu, Z.; Liu, Y.; Yang, C. J.; Yan, H. *Angew. Chem., Int. Ed.* **2016**, *55*, 7483−7486.
(31) Xie, S. B.; Dong, Y. W.; Yuan, Y. L.; Chai, Y. Q.; Yuan, R. *Anal. Chem.* **2016**, *88*, 5218−5224.
(32) Dai, J. Y.; He, H. F.; Duan, Z. J.; Guo, Y.; Xiao, D. *Anal. Chem.* **2017**, *89*, 11971−11975.
(33) Fan, D. Q.; Zhu, X. Q.; Zhai, Q. F.; Wang, E.; Dong, S. J. *Anal. Chem.* **2016**, *88*, 9158−9165.
(34) Zhou, W. J.; Zhu, J. B.; Fan, D. Q.; Teng, Y.; Zhu, X. Q.; Dong, S. J. *Adv. Funct. Mater.* **2017**, *27*, 1704092.
(35) Hou, T.; Li, W.; Liu, X. J.; Li, F. *Anal. Chem.* **2015**, *87*, 11368−11374.
(36) Xiong, E. H.; Li, Z. Z.; Zhang, X. H.; Zhou, J. W.; Yan, X. X.; Liu, Y. Q.; Chen, J. H. *Anal. Chem.* **2017**, *89*, 8830−8835.
(37) Xuan, F.; Fan, T. W.; Hsing, I. M. *ACS Nano* **2015**, *9*, 5027−5033.

DOI: 10.1021/acs.analchem.8b05407
Anal. Chem. 2019, 91, 3561−3566